An AI Approach in Radioactive Source Localization by a Network of Small Form Factor CZT Sensors

Aristotelis Kyriakis*
Institute of Nuclear and Particle Physics, NCSR "DEMOKRITOS"
15341, Agia Paraskevi, Attica, Greece
kyriakis@inp.demokritos.gr

Konstantinos Karafasoulis*
Hellenic Army Academy
16673, Vari, Attica, Greece
ckaraf@gmail.com

ABSTRACT

We present a small form factor ($0.5cm^3$) static CZT sensor network consisted of a number of Non- Directional Detectors (NDD) capable to localize a stationary radiation source in 3D. The localization is performed with a fusion algorithm based on AI techniques. The algorithms are based on Multilayer Perseptron Neural Network (MLP) and Gradient Boosted Decision Trees (BDTG). They have been trained using simulated data produced by the SWORD simulation software based on Geant4 framework. The localization efficiency of the algorithms was verified with experimental data taken in our laboratory using a ^{137}Cs source of $180\mu Ci$. The localization resolution of the order of 10cm to 15cm has been archived in Vertical and Horizontal directions respectively and of the order of less than 20cm in the depth direction within a monitored volume of 5m x 2.8m x 2m .

CCS CONCEPTS

• **Computer systems organization** → **Embedded systems**; *Redundancy*; Robotics; • **Networks** → Network reliability.

KEYWORDS

Neural networks, Boosted Decision Trees, CZT sensors, Radiation, Source Localization

1 INTRODUCTION

In the new era of homeland security there is a growing concern regarding the possession and the potential use of radiological materials by terrorist groups usually in the form of a radiological dispersion device (RDD), also known as "dirty bomb". Since the defended areas from such a threat may not have specific entrance and exit points, the problem of how to localize and identify a radioactive source in an open area should be investigated. The detection has to overcome a variety of uncontrollable factors, such as the presence of benign sources, time and space varying background noise, and obstacles that may occlude signal from sources. An overview of the related work in this subject can be seen in section 2. In this work we focus on the localization of stationary radioactive sources using a network of small form factor static spectroscopic detectors (Non-Directional Detectors - NDD) realized using CZT crystals. This network was used as a verification platform for the set of the developed localization algorithms. The capabilities of the above NDD network to localize radioactive sources were investigated using simulated data produced by GEANT4 [4] software via the SWORD (SoftWare for Optimization of Radiation Detectors) package [23]. Then a series of verification tests were performed using experimental data collected by a locally developed data acquisition system from the CZT sensor network realized in our lab. The localization algorithms were based on machine learning techniques, such as Neural Networks (MLP) and Boosted Decision Trees (BDT).

2 RELATED WORK

The radiation localization problem has been studied extensively in the last years in the framework of homeland security. Localization algorithms evolved from single detector ones to sensor networks and to mobile sensor networks. The complexity of the problem also evolved from the localization of single radiation source to many radiation sources and to mobile radiation sources.

The single detector algorithms are based on the determination of a threshold on the count rate of the detector [14]. The threshold is unusually defined as a multiple of the estimated background count rate. Although such an algorithm can detect the presence of a radiation source, it lacks the ability to efficiently localize it. This limitation has been surpassed with the use of radiation sensor networks that have the ability to record the radiation information (e.g. counts or spectra) for the same time window. Radiation information is then fused in order to localize the radiation source. Several fusion algorithms have been proposed by various researchers.

The Ratio of Square-Distance (RoSD) algorithm [12] uses information provided by 3 sensors to estimate the location of the source. The algorithm suffers from the estimation of a second position of the radiation source together with the real position, often mentioned as phantom estimate. The origin of the problem lies in the inability of the algorithm to distinguish a strong source far away from the sensors from a weaker source located in a shorter distance. A more elaborate approach that resolves the above ambiguity involves the deployment of more than 3 sensors. However, the method is still prone to noisy data in the real world scenario, where it could not localize the source at all.

The Maximum Likelihood Estimation (MLE) algorithm has been proposed by [5], [3], [10] for the localization of the source and the estimation of its activity in 2D. The method handles the assessment of the source parameters as a multidimensional minimization problem, where the function to be minimazed is the error between the recorded and estimated sensor readings. The method can converge on local minima, which leads to the detection of phantom sources.

*Both authors contributed equally to this research.

AINST2020, September 02–04, 2020, Athens, Greece

A faster algorithm with respect to the MLE has been proposed by S. Nageswara et al [20], the Mean-of-Estimator (MoE). The algorithm evaluates the mean of all candidate source estimates. However,it is prone to large source localization errors when phantom sources are included in the sample.

The complexity of the localization problem increases at the presence of multiple radiation sources. In such a scenario the number of the radiation sources is not known and it must be estimated from the data. This can be done by applying a statistical test which evaluates the most probable number of sources prior to the localization algorithm.

Bayesian algorithms have been proposed in [22], [7], [13], [8] for the source localization problem. The source parameters i.e. the activity of the source and its location are estimated using a set of observables, the sensor readings. To do so the algorithm computes the posterior probability distribution based on an estimated prior distribution. However, the prior estimates can not be easily determined in real world scenarios where the background can not be modeled as a Poisson distribution due to the presence of obstacles. Also source localization has been proposed by a Delayed Rejection Adaptive Metropolis (DRAM) algorithm [19] .

In addition a particle filter approach has been used in [18], [11],[17] in order to estimate the source location. In this algorithm a large number of random samples of source activity and location (called particles) have been used to estimate the probability distribution function (*PDF*). For each particle the expected radiation readings of the sensors are estimated and the probability to record a specific set of measurement is calculated. The accumulation of more measurements causes the expectation of particles to converge to the real source location and activity. Although, this approach works well for single radiation source the complexity of the algorithm increases exponentially with the number of sources [9].

The approach of using static radiation sensors is good when the target is the protection of a restricted monitoring area. In contrast, when the target is the protection of a big city this approach is not sufficient. Thus, mobile sensor networks have been proposed in [16] for detecting people carrying radioactive material and in [24] for detecting radioactive sources in urban areas 2019.

However, in this work we focus on an AI approach for the radioactive source localization based on MVA techniques.

3 NON DIRECTIONAL DETECTORS SIMULATION

3.1 Geometrical Setup of the Simulation

Detailed simulation has been used to study the ability of the NDD network to localize a radioactive source within a volume of $28m^3$. A model of 5 CZT spectroscopic sensors in cruciform topology (" 5 Sensor Cross topology ") having an active volume of $0.5cm^3$ each, has been irradiated by a ^{137}Cs source having an activity of $1mCi$ for $\Delta t = 45sec$ in the absence of NORM background. The inter-sensor distance in the horizontal axis was set to $2.5m$ whilst the vertical inter-sensor distance was set to $1.4m$. This setup was selected to match with our experimental hall specification. The source has been placed at various positions (figure 1) i.e. within parallel planes at distances between $40cm$ to $200cm$ away from the sensor plain in steps of $40cm$. The energy response of the 5 CZT sensors was recorded for a grid of 3000 different source position points per layer.For simplicity we simulated source positions in planes parallel to the detectors plain, however during the training phase the events (source position) were randomly picked up from the above sample.

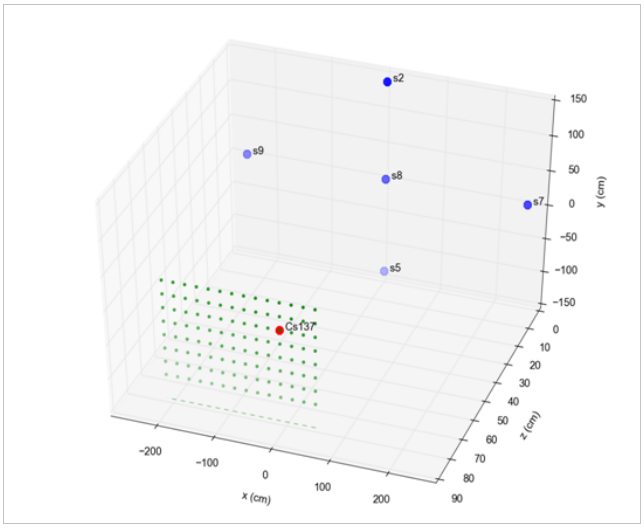

Figure 1: Simulation setup of the " 5 Sensor Cross topology " (S2, S5, S7, S8, S9) in blue. The energy response of the sensors has been recorded when a radioactive source i.e.^{137}Cs (in red) has been placed in various position (in green) at planes parallel to the sensor plane.

3.2 MVA techniques description

Although the energy spectra, of each sensor is recorded, for the same time window Δt this work uses only the total recorded counts in each sensor (N). This is done to increase the sensitivity of the sensors by taking into account not only the photo-peak information but the scattered radiation as well. The localization of the radiation source algorithms have been designed to handle sources independent of their activity, by using the sensor with the maximum response (maximum number of counts) as a normalization factor for all the sensors. In general: $N \simeq Ae^{-\mu r}/r^2$, where A is related to the source activity and the sensor efficiency, μ is the attenuation coefficient and r is the distance between radiation source and sensor. It is obvious that without normalization the algorithms could be biased by the source activity. Thus the normalization we performed to the maximum recorded counts is mandatory to get rid off the dependence of the source activity. The set of the recorded normalized counts by all sensors, is the set of the input variables to the Multivariate Analysis algorithms (MVA) and it defines a single event. The TMVA [6] toolkit has been used for the MVA methods through the ROOT [2] framework.

The basic steps of our approach are the following:

- Normalize Sensor Readings to the sensor with the maximum recording during the same time window.
- Use MVA techniques to estimate independently the Horizontal (X), Vertical (Y) and Depth (Z) position of the source by

taking into account the normalized sensor counts.We have chosen three independent models one for each space coordinate and not one model with two or three position outputs since the number of simulated events is not sufficient large to support this exercise.

For the second step above the following regression techniques have been evaluated:

- Multi Layer Persepton Artificial Neural Network (MLP),
- Gradient Boosted Decision Trees (BDTG)

Both of the above regression techniques are supported by the TMVA [6] toolkit.

3.3 MLP method

Neural Networks are used in a variety of tasks such as pattern recognition, computer vision, speech recognition and regression problems. They consist of interconnected nodes, called neurons, which are organized in layers. Signals travel from the first layer (input), to the last layer (output). Their internal layers are known as hidden layers. In this article the Multi-Layer Percepton Artificial Neural Network (MLP) realized in the TMVA package has been used (figure 2). During the learning phase the network was supplied with $N_{training} = 12000$ training and $N_{test} = 3000$ test samples from the simulated data (the normalized sensor counts) where the output of the network (the radiation source coordinate) is known. The neuron weights are adjusted by the BFGS [21] algorithm and *tanh* as activation function. The parameters used in MLP can be seen in Table 1.

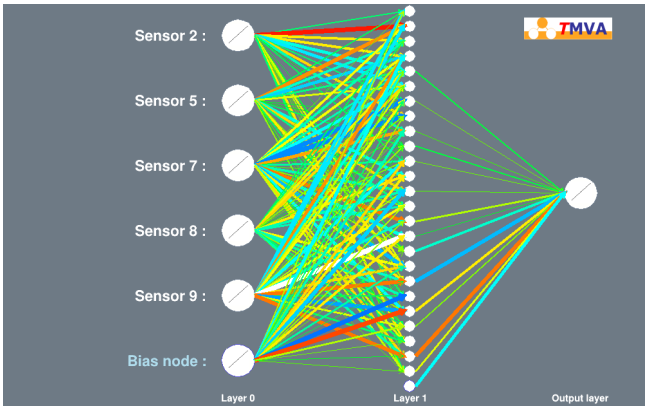

Figure 2: Schematic of the neural network with 5 input nodes(the normalized sensor counts), 1 hidden layer with 26 nodes and one output node for the Source Coordinate estimation.

The linear correlation matrix of the input variables is shown in figure 3 where a clear lack of correlation is observed. In figure 4 the successful convergence test is shown where no overtraining is observed since the test line (blue dot line) lies above the training line (red line).

Table 1: Neural Network Parameters

Neural Network Parameter	Value
Number of Training Samples	12000
Number of Testing Samples	3000
Number of Cycles(Epochs)	1000
Hidden Nodes	26
Training Method	BFGS
Activation Function	tanh
Convergence	$1E^{-6}$

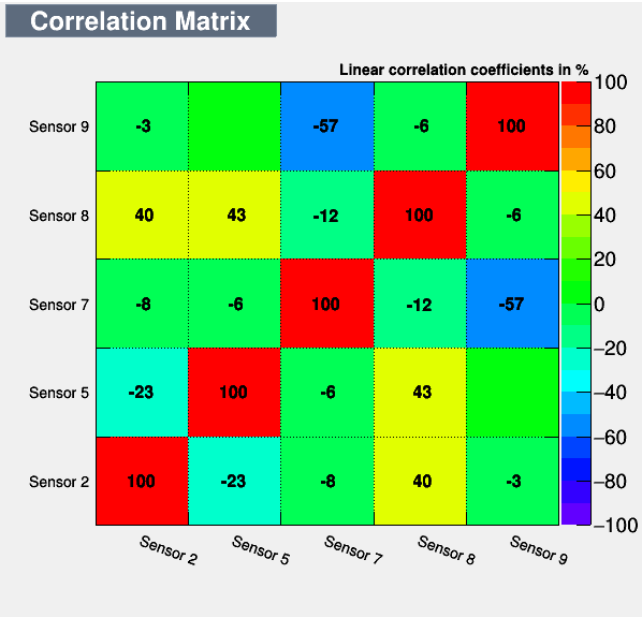

Figure 3: The linear correlation matrix of the input variables for the MLP method.

3.4 Gradient Boosted Decision Trees (BDTG) method

Decision Trees started to play an important role in discriminating data in two classes when a set of input variables provides enough information to separate the data after a series of cuts in the input variables. Usually data provided by simulation are used to train the Decision Tree, where class identification is known a priori. However, decision trees suffer from instabilities depending on the data training set. This problem has already been solved [15] by creating a forest of trees, where each misclassified event is reweighted (boosted) in order to be used in the next tree in the forest. A scoring algorithm that spans through all trees in the forest defines the final class decision for the event. A similar approach is used if instead of a classification, we have to deal with a regression problem, where the end leaf defines the achieved value (figure 5). The parameters of the Gradient BDT used in our case can be seen in Table 2.

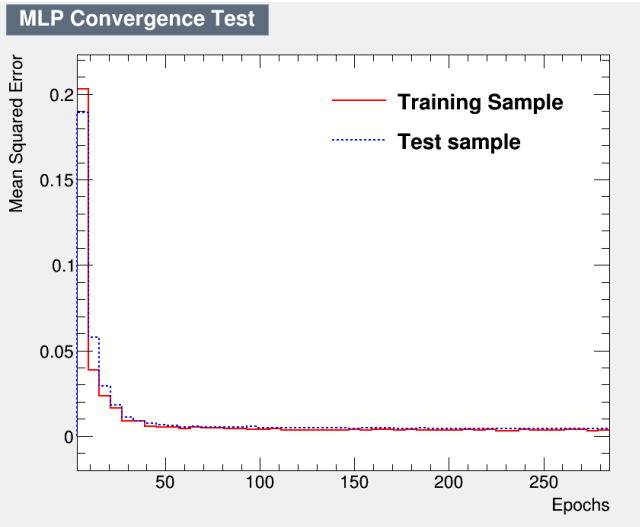

Figure 4: The MLP convergent test. No overtraining is observed since the test line (blue dot line) lies above the training line(red line)..

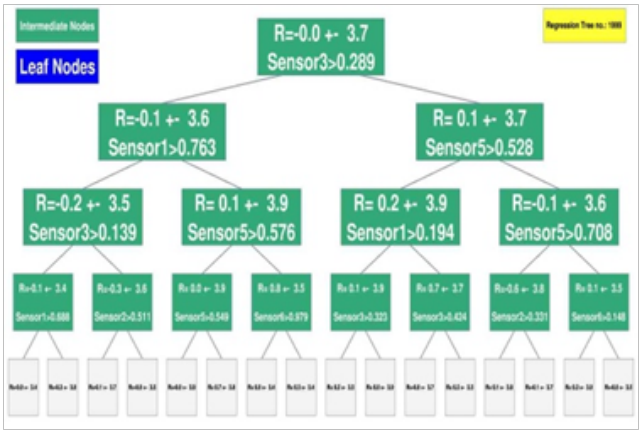

Figure 5: Schematic of the Gradient BDT Boost Type for the Source Coordinate estimation.

4 EVALUATION OF MVA ALGORITHMS

After the training of both the MLP and BDTG methods, the produced weights were evaluated with simulated samples from ^{137}Cs source, not previously seen in the training phase.

4.1 Evaluation with ^{137}Cs source

An evaluation sample was produced with a ^{137}Cs source at a distance of 1m away from the sensor plain of the same activity ($1mCi$) and for the same radiation exposure time ($\Delta t = 45sec$) as the training sample, using the SWORD package. This sample was not used during the training phase. Figure 6 refers to the "5 Sensor Cross topology" and shows: (a),(c) the horizontal source position accuracy (estimated horizontal coordinate minus its true value) by the MLP method and BDTG method respectively as a function of the corresponding true horizontal coordinate, (b),(d) the horizontal source position accuracy from the MLP method and from the BDTG method respectively. As can be seen the horizontal accuracy is almost flat with respect to the true source horizontal coordinate except some small deviation towards the edges of the monitoring volume. It is well centered to zero with resolution (the RMS of the accuracy distribution) of the order of $10cm$ in accordance to our grid segmentation ($10cm$) of the source locations used in the training. Figure 7 refers to the "5 Sensor Cross topology" and shows: (a),(c) the vertical source position accuracy (estimated vertical coordinate minus its true value) by the MLP method and BDTG method respectively as a function of the corresponding true vertical coordinate, (b),(d) the vertical source position accuracy from the MLP method and from the BDTG method respectively. It can be seen the vertical accuracy is almost flat with respect to the true source vertical coordinate except some small deviation towards the edges, it is well centered around zero with resolution of the order of $9cm$ close to our grid segmentation ($5cm$) of the source locations used in the training.

Table 2: Gradient BDT Parameters

BDT Parameter	Value
Number of Training Samples	12000
Number of Testing Samples	3000
Number of Trees	2000
Granularity	20
Maximum Depth	4
Boost Type	Gradient
Separation Type	Regression Variance
Prune Method	Cost Complexity

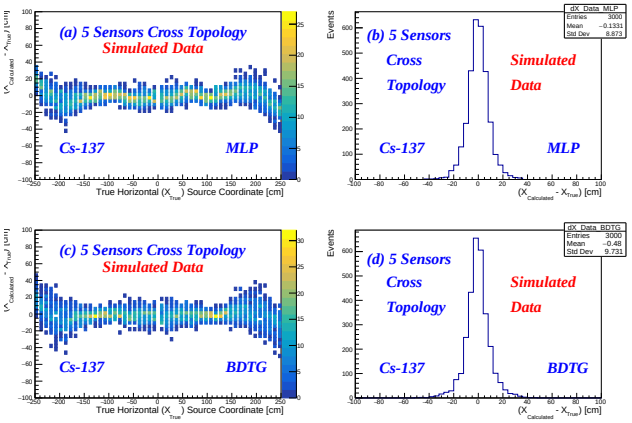

Figure 6: Simulated "5 Sensors Cross topology" with a ^{137}Cs Source ($1mCi$) at 1m from sensor plain that radiated for $45sec$. Horizontal source position accuracy by the MLP method (a) and by the BDTG method (c) vs the true horizontal source coordinate. Horizontal source position accuracy by the MLP method (b) and by the BDTG method (d).

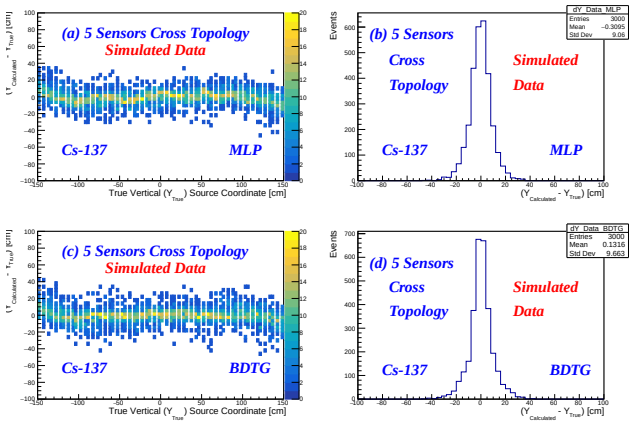

Figure 7: Simulated "5 Sensors Cross topology" with a ^{137}Cs Source ($1mCi$) at 1m from sensor plain that radiated for $45sec$. Vertical source position accuracy by the MLP method (a) and by the BDTG method (c) vs the true vertical source coordinate. Vertical source position accuracy by the MLP method (b) and by the BDTG method (d).

Figure 8 refers to the "5 Sensor Cross topology" and shows: (a) the depth source position accuracy by the MLP method at the source distance of 1m from the sensor plain and (b) the corresponding depth source position accuracy by the BDTG method. A small bias at the central value with a resolution of the order of $12cm$ was observed less to our grid segmentation ($40cm$) of the source locations used in the training

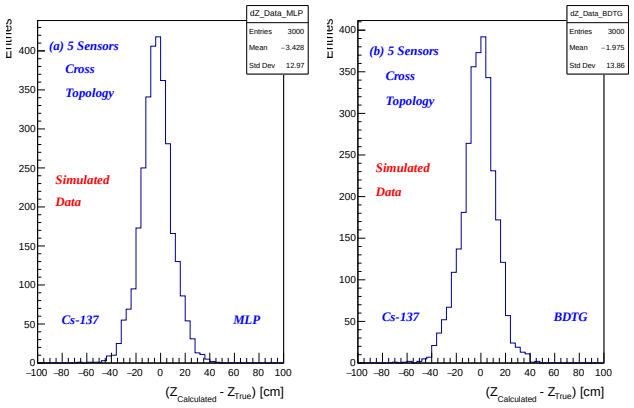

Figure 8: Simulated "5 Sensors Cross topology" with a ^{137}Cs Source ($1mCi$) at 1m from sensor plain that radiated for $45sec$ (a) the depth source position accuracy from the MLP method at the source distance of 1m from the sensor plain and (b) the corresponding depth source position accuracy from the BDTG method.

5 EXPERIMENTAL SETUP

5.1 Source Position Platform

For the verification of the data fusion algorithms a test- bed was setup using CZT detectors purchased by RITEC[25]. A 3-D step-motor rail system that positions a radioactive source in predefined position has been developed and installed in the testbed area.(the RMS of the accuracy distribution) The 3-D step motor system is controlled by an Arduino microcontroller [1]. A software GUI written in java controls and sends the appropriate commands to Arduino microcontroller in order to position the radiation source in the desired position.

5.2 DAQ System

A locally developed Data Acquisition System (DAQ) has been used to collect the spectra for the various radioactive source positions. The DAQ system consists of two software components.

The main tasks of the client are :

- to connect to the sensor and control it. To send commands to the sensor and receive the responses.
- to accept control connections from the server. Through these connections, it receives commands and sends back the responses.
- to send measurement data to the server.

The main tasks of the server are:

- to send commands to the clients.
- to provide feedback during the execution of the commands.
- to receive and store measurements from the clients in a database.
- to allow retrieval of past measurements for analysis.

The client follows a layered structure. Each layer communicates only with the layer above or below it. This layered architecture achieves low coupling between the client logic and the sensor type. Adding support for a new type of sensor requires only creating a new sensor manager implementation for the specific sensor. In addition the server communicates through the command controller layer while the sensor communicates through the sensor manager implementation corresponding to its type. The software for the fusion node utilizes web technologies [26] which make it possible for the sensors, the fusion node, and the operator to be at different locations. A session is a series of measurements performed by a number of sensors over a specific period of time. For each session we can define the type of the radiation source (or background), the date and time that the measurement started and the configuration. By the term configuration we mean the number of measurements that every sensor will perform and the duration of each one of these measurements. A small paragraph of text can also by recorded for each session containing further details.

5.3 Sensor Energy Response

In figure 9 an indicative response of the five sensors $S2(top)$, $S8(central)$, $S5(bottom)$, $S7(right)$ and $S9(left)$ is shown after $3min$ of irradiation with a $180\mu Ci$ ^{137}Cs source and after background subtraction for a central source position. For each source position the sensors spectrum was saved every $10sec$ of acquisition time, resulting in 18 spectrum stamps during the $3min$ of total

acquisition time. The source is located at a distance $120cm$ away from the sensor plain inside our test volume. Clear evidence of the presence of the ^{137}Cs source is the photo-peak around $662keV$ seen more pronounced by sensors, $S9$, $S8$, $S7$ and $S5$.

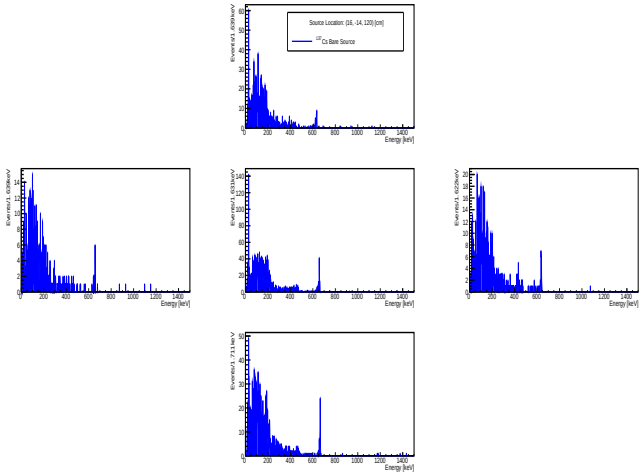

Figure 9: The response after $3min$ of exposure at a $180\mu Ci$ ^{137}Cs source of the five sensors $S2(top)$, $S8(central)$, $S5(bottom)$, $S7(right)$ and $S9(left)$ after background subtraction. Clear evidence of the presence of the ^{137}Cs source is the photo-peak around $662keV$ and the $X-ray$ peak of $32keV$.

The energy spectra received are consisted of two parts: (a) the photo-peak and (b) the continuum part of the spectrum. In the case of the unshielded sources studied in our case (this can be verified by the presence of the $X-ray$ peak around $32keV$ seen in the spectra plot and more pronounced by sensor $S8$), the continuum part of the spectrum is mainly due to Compton scattering in the surrounding the detector material.

6 ALGORITHM VERIFICATION WITH EXPERIMENTAL DATA

The weights produced from the simulated data were used to evaluate the algoritms with experimental data. The source spatial accuracy estimated by the "5 Sensor Cross Topology" system is presented in figures 10 (Horizontal accuracy), 11 (Vertical accuracy) and 12 (Depth accuracy) respectively. The Horizontal and Vertical resolution (the RMS of the accuracy distribution) is of the order of $10cm$ to $15cm$ in accordance to the simulation results but the Depth resolution is worse with a pronounced bias in the mean value as can be seen in figure 13, where the mean depth accuracy is plotted as a function of the true depth source coordinate. A clear bias of almost the almost the same level is observed and this is subtracted from the estimated depth value to produce the plot seen in figure 12. This systematic bias is mainly due to the scattering material all around the experimental area that reduces the total counts recorded by the sensors and thus giving the impression that the source is further that it is in reality. This scattering was not taken into account in the simulation and thus the produced weights do not contain this information. An easy solution to this problem was to calculate the above correction (shown in figure 13) and subtract it from the estimated depth coordinated. Another solution is to fine tune the model by including real data in the training phase giving in this way the missing information concerning the signal attenuation due to scattering in the surrounding material.

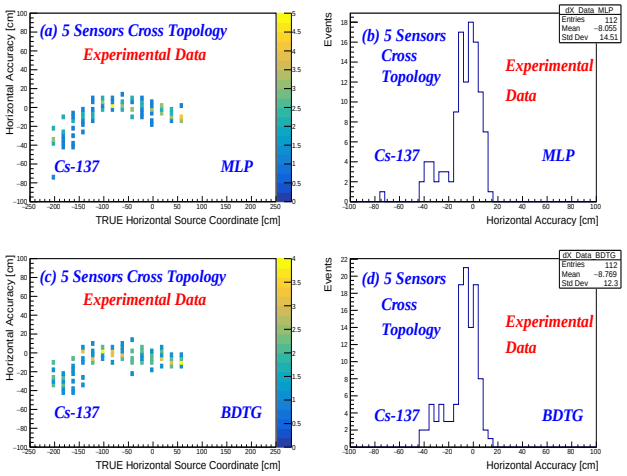

Figure 10: Experimental "5 Sensors Cross topology" with a ^{137}Cs Source ($180\mu Ci$) at $1.2m$ from sensor plain that radiated for $3min$. Horizontal source position accuracy by the MLP method (a) and by the BDTG method (c) vs the true horizontal source coordinate. Horizontal source position accuracy by the MLP method (b) and by the BDTG method (d).

7 CONCLUSIONS

The ability of a sensor network consisting of five small form factor CZT sensors having a co-planar topology to estimate a radioactive source position in 3D has been evaluated using supervised machine learning techniques on fully simulated data samples. The algorithms have been verified by a series of experiments, where the CZT sensor network has been irradiated by a ^{137}Cs Source of $180\mu Ci$. A localization accuracy within a volume of 5m x 2.8m x 2m of $10cm$ to $15cm$ in vertical and horizontal source coordinates respectively has been achieved after an exposure time of $3min$ while the depth is estimated with a resolution of less than $20cm$ but with a bias in the accuracy mean value that can be easily corrected.

8 ACKNOWLEDGMENTS

This research has been funded by NATO (SfP-984705) SENERA project.

REFERENCES

[1] Arduino 2020. *Arduino Uno Homepage.* https://www.arduino.cc/
[2] R. Brun and F. Rademakers. 1997. ROOT - an object oriented data analysis framework. *Nucl. Instrum. Meth. Phys. Res. A* 389, 81 (1997).
[3] B. Deb. 2013,. Iterative estimation of location and trajectory of radioactive sources with a networked system of detectors,. *IEEE Trans. Nucl. Sci.*, 60, 2 (2013,), pp. 1315–1326,. https://ieeexplore.ieee.org/stamp/stamp.jsp?tp=&arnumber=6485009
[4] Agostinelli et al. 2003,. GEANT4 - a simulation toolkit,. *Nucl. Instrum. Meth. A*, 506 (2003,), pp. 250,.

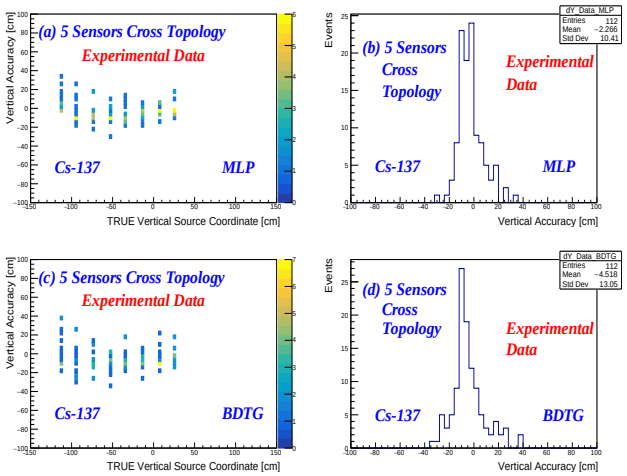

Figure 11: Experimental "5 Sensors Cross topology" with a ^{137}Cs Source ($180\mu Ci$) at $1.2m$ from sensor plain that radiated for $3min$. Vertical source position accuracy by the MLP method (a) and by the BDTG method (c) vs the true vertical source coordinate. Vertical source position accuracy by the MLP method (b) and by the BDTG method (d).

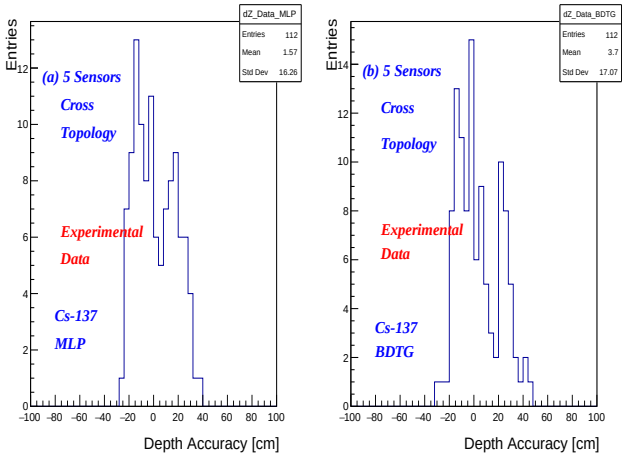

Figure 12: Experimental "5 Sensors Cross topology" with a ^{137}Cs Source ($180\mu Ci$) at $1.2m$ from sensor plain that radiated for $3min$. Depth source position accuracy (after bias subtraction) by the MLP method (left) and by the BDTG method (right).

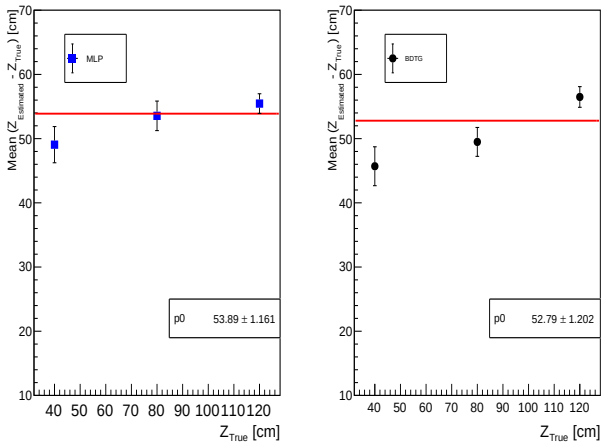

Figure 13: A clear bias of almost the same level is observed in the estimated source depth as a function of the true source depth for both methods i.e MLP (left) and BDTG (right). This corrections should be subtracted from the estimated source depth.

[5] A. Gunatilaka et al. 2007,. On localisation of a radiological point source,. *Proceedings of Conference on Embedded Networked Sensor Systems (SenSys)*, IEEE (2007,), pp. 236–241,. https://ieeexplore.ieee.org/stamp/stamp.jsp?tp=&arnumber=4252508

[6] A. Hoecker et al. 2007. TMVA - Toolkit for Multivariate Data Analysis. *PoS ACAT*, 040 (2007). arXiv:physics/0703039.

[7] A. H. Liu et al. 2011,. Sensor networks for the detection and tracking of radiation and other threats in cities,. *Information Processing in Sensor Networks (IPSN), 2011 10th International Conference*, IEEE (2011,), pp. 1–12. https://ieeexplore.ieee.org/stamp/stamp.jsp?tp=&arnumber=5779060

[8] C. Farinetto et al. 2020,. A. Poisson source localization on the plane: change-point case,. *Ann Inst Stat Math* , 72 (2020,), pp. 675–698,. https://doi.org/10.1007/s10463-018-00704-0

[9] Chris Kreucher et al. 2005,. Multitarget tracking using the joint multitarget probability density,. *Proceedings of IEEE Transactions on Aerospace and Electronic Systems*, 41„ (4), (2005,), pp. 1396–1414. https://ieeexplore.ieee.org/stamp/stamp.jsp?tp=&arnumber=1561892

[10] E. Bai et al. 2015,. Maximum Likelihood Localization of Radioactive Sources Against a Highly Fluctuating Background,. *IEEE Trans. Nucl. Sci.*, 62, 6 (2015,), pp. 3274–3282,. https://ieeexplore.ieee.org/stamp/stamp.jsp?tp=&arnumber=7348750

[11] J Cook et al. 2020,. Particle Filtering Convergence Results for Radiation Source Detection,. *arXiv preprint: arXiv:2004.08953*, (2020,). https://arxiv.org/pdf/2004.08953.pdf

[12] J-C Chin et al. 2008,. Accurate localization of low-level radioactive source under noise and measurement errors,. *Information, Decision andControl, 2007. IDC 201907*, (2008,), pp. 183–196,. https://dl.acm.org/doi/abs/10.1145/1460412.1460431

[13] K. D. Jarman et al. 2011,. Bayesian Radiation Source Localization,. *Nuclear Technology*, 175, 1 (2011,), pp. 326–334,. https://www.tandfonline.com/doi/pdf/10.13182/NT10-72?needAccess=true

[14] K. M. Chandy et al. 2010,. Models and algorithms for radiation detection. Modeling and Simulation,. *Workshop for Homeland Security*, (2010,), pp. 1–6,. http://citeseerx.ist.psu.edu/viewdoc/download?doi=10.1.1.190.7783&rep=rep1&type=pdf

[15] L. Mason et al. 1999. Boosting Algorithms as Gradient Descent,. *MIT Press, Advances in Neural Information Processing Systems* 12, 512 (1999).

[16] M. Chandy et al. 2008,. Networked sensing systems for detecting people carrying radioactive material,. *Networked Sensing Systems, INSS 2008, 5th International Conference*, IEEE, (2008,), pp. 148–155. https://ieeexplore.ieee.org/stamp/stamp.jsp?tp=&arnumber=4610916

[17] N. Pinkam et al. 2020,. Informative Mobile Robot Exploration for Radiation Source Localization with a Particle Filter,. *2020 Fourth IEEE International Conference on Robotic Computing (IRC),Taichung, Taiwan*, (2020,), pp. 107–112,. https://ieeexplore.ieee.org/stamp/stamp.jsp?tp=&arnumber=9287935

[18] N. Rao et al. 2015,. Network algorithms for detection of radiation sources,. *Nucl. Instum. Meth. in Physics Research Section A: Accelerators, Spectrometers, Detectors and Associated Equipment*, 784, (2015,), pp. 326–331,. https://doi.org/10.1016/j.nima.2015.01.037

[19] P. R. Miles et al. 2021,. Radiation Source Localization Using Surrogate Models Constructed from 3-D Monte Carlo ,. *Transport Physics Simulations, Nuclear Technology*, 207, 1 (2021,), pp. 37–53,. https://www.tandfonline.com/doi/pdf/10.1080/00295450.2020.1738796?needAccess=true

[20] S. Nageswara et al. 2008,. Localization under random measurements with application to radiation sources,. *Proceedings of the 11th International Conference on*

Information Fusion (FUSION), IEEE (2008,). https://ieeexplore.ieee.org/stamp/stamp.jsp?tp=&arnumber=4632200

[21] Roger Fletcher. 1987. *Practical methods of optimization* (2nd ed.). John Wiley and Sons, NJ, USA.

[22] M. R. Morelande and B. Ristic. 2009,. Radiological source detection and localisation using Bayesian techniques,. *Signal Processing, IEEE Transactions,* 57,, (11), (2009,), pp. 4220–4231. https://ieeexplore.ieee.org/stamp/stamp.jsp?arnumber=5153354

[23] Oak Ridge National Laboratory 2020. *RSICC CODE PA CKAGE CCC-7676,*. http://www-rsicc.ornl.gov/codes/ccc/ccc7/ccc-767.html

[24] et al. P. Tando. 2016,. Detection of radioactive sources in urban scenes using Bayesian Aggregation of data from mobile spectrometers,. *Information Systems,* 57, (2016,), pp. 195–206. https://doi.org/10.1016/j.is.2015.10.006

[25] RITEC 2020. *Gamma-Radiation CdZnTe Microspectrometer.* http://www.ritec.lv/files/uspec/R_uSPEC_A4_v5b.pdf

[26] WildFly 2020. *WildFly a flexible, lightweight, managed application runtime.* https://www.wildfly.org/

[27] Jifu Zhao and Clair J. Sullivan. 2019,. Detection and parameter estimation of radioactive sources with mobile sensor networks,. *Radiation Physics and Chemistry,,* 155, (2019,), pp. 265–270. https://www.sciencedirect.com/science/article/pii/S0969806X17307752